10-19-2023 12:00 PM

Quantifying Neuromelanin Content Across Varying Magnetic Field Strengths: A Comparative Analysis

Laiba Rizwan, *Western University*

Supervisor: Morton, J. Bruce, *The University of Western Ontario*

A thesis submitted in partial fulfillment of the requirements for the Master of Science degree in Neuroscience

Abstract

Neuromelanin (NM) is an insoluble dark pigment molecule that is found in the substantia nigra of the human brain. Due to its paramagnetic nature, NM can be imaged using MRI in the form of neuromelanin sensitive contrast. This method, known as Neuromelanin Sensitive Magnetic Resonance Imaging (NM-MRI) allows non-invasive imaging of the human substantia nigra through its by-product, NM. NM-MRI research has been mostly done using lower field strength (3 or 1.5 Tesla) MRI scans. The advent of high field strength imaging, e.g., 7 Tesla (7T) provides the opportunity to study neuromelanin production sites with higher spatial resolution and enhanced detail. Since NM-MRI research has not been conducted with high field strength imaging platforms, it is unknown whether the techniques used for quantifying NM at a lower field strength reliably extend to a high field strength platform. In the absence of this information, it is impossible to establish whether these two sequences generate the same estimates of NM. Thus, before it is possible to harness the advantages of high field strength imaging, it is critical to investigate the convergence of NM-MRI signal between 3T and 7T NM-MRI. The current study employs a within-subjects design to answer this question. Neuromelanin sensitive images were obtained from 28 healthy adult participants at both 3T and 7T. NM images were segmented both manually and with the help of a standard atlas. NM in the substantia nigra was quantified in the form of Contrast to Noise Ratio (CNR). Spearman's rank order correlations assessed statistical dependence between the ranking of participant CNR values at 3T and 7T. We found that CNR values at 3T predicted those at 7T when standard deviation (as opposed to the mean) of the background region was used for defining noise. In addition, CNR values didn't increase with an increase in field strength. In fact, CNR values at 7T were lower as compared to 3T. This effect was mainly due to a disproportionate increase in noise at 7T. An increased susceptibility noise is

a common trade-off for better contrast associated with high field strength imaging. We discuss our findings and comment on the utility of employing high field strength NM- MRI.

Keywords: Neuromelanin, neuromelanin sensitive contrast, contrast to noise ratio, manual segmentation, atlas-based segmentation, substantia nigra, crus cerebri

Summary for Lay Audience

Dopamine is a neurotransmitter that involved in learning, reward processing, and motivation. A by-product of normal dopamine metabolism in humans, neuromelanin has recently been used to gain a deeper understanding of the human dopamine system. Because of its magnetic nature, neuromelanin gives a unique signal when imaged using a family of magnetic resonance imaging (MRI) sequences. These sequences generate neuromelanin sensitive contrast but has only been investigated in low field strength MRI. The advent of high field strength MRI has advanced the visualization of the brain because of its superior spatial resolution. Leveraging the benefits of high field strength imaging bears the promise of furthering our current understanding of neuromelanin and the dopamine system. However, before these benefits can be harnessed for neuromelanin research, it is critical to test if the image processing techniques and statistical analyses used for quantifying neuromelanin signal at low field strength provide reliable estimates of neuromelanin quantification at a high field strength imaging platform. Thus, the current research aims to investigate if estimates of neuromelanin converge between 3 Tesla (low field strength) and 7 Tesla (high field strength) MRI scans. For this purpose, we scanned participants using both 3T and 7T MRI scans to obtain neuromelanin sensitive images. Images were analyzed using different techniques to assess NM-MRI signal strength in neuromelanin rich areas, as compared to areas with no neuromelanin. In this paper, we discuss our findings and comment on the utility of employing high field strength imaging for studying neuromelanin signal.

Dedication

To my mentor, Mike.

Acknowledgments

First and foremost, I'm deeply grateful to my supervisor, Prof. J Bruce Morton for being awesome! Thank you for letting me carve my path and for the skill building opportunities you gave me. I appreciate and admire your patience and approachable demeanor. Thank you for taking the time to mentor me despite having a million things on the go, for showing pride in my accomplishments and making me feel like a cherished member of your lab group. I am truly blessed and fortunate to have met and learnt from you. Your unwavering support and faith mean the world to me.

I am grateful to members of my advisory committee, Profs. Emma Duerden, Andrea Soddu, Ryan Stevenson for their valuable feedback towards enhancing the quality of my work. My sincerest gratitude to Dr. Hagen H. Kitzler and Lisa Hösel for taking the time to create manually segmented masks of our dataset. I am also grateful to Prof. Clifford Cassidy for providing us with the atlases he used in his work on the topic. This project wouldn't have been possible without your hard work and dedication.

A special thank you to members of the Cognitive Development and Neuroimaging Lab: Aria, Bea, Kaycee, Amira, Adam, and Samm for their time, enthusiasm, and support. Thank you for laughing at my jokes, listening to my rants, and walking beside me on the grad school journey. I couldn't have asked for a more supportive research team.

An honorable mention to my remarkable friends: Sakina, Massar, Asil, Insiya, Taimiyyah, and Anuj for being the most amazing friends anyone can ever ask for. I am eternally indebted to you for adding life to my days, for epitomizing loyalty and comradery, and for bestowing on me the gift of your friendship.

Finally, a huge shoutout to my extraordinary family. My dearest Mama and Baba, my rockstar siblings: Jairy, Alina, Hamna, Hania, Abdullah, and Omair Bhai. I love you more than words can say. Thank you for being my biggest cheerleaders, the wind beneath my wings. Home is where you are!

Table of Contents

List of Figures

List of Abbreviations

NM	Neuromelanin
MRI	Magnetic Resonance Imaging
NM-MRI	Neuromelanin Sensitive Magnetic Resonance Imaging
SN	Substantia Nigra
CC	Crus Cerebri
CNR	Contrast to Noise Ratio
ROI	Region of Interest
3T	Three Tesla
7T	Seven Tesla
SI	Signal Intensity
LC	Locus Coeruleus
SPM	Statistical Parametric Mapping
RMS	Root Mean Square
SNR	Signal to Noise Ratio
FOV	Field of View
TE	Echo Time
TR	Repetition Time
TI	Inversion Time
GRE	Gradient Echo Sequence
MPRAGE	Magnetization-Prepared Rapid Acquisition Gradient Echo.
PET	Positron Emission Tomography
GRAPPA	GeneRalized Autocalibrating Partial Parallel Acquisition

MNI	Montreal Neurological Institute
SD	Standard Deviation

1 Introduction

1.1. Human Dopaminergic System

The human dopaminergic system supports a plethora of physiological, psychological, and behavioural processes including executive functioning (Monchi et al., 2016), reward processing (McClure et al., 2004), mood regulation (Dunlop & Nemeroff, 2007; Radwan et al., 2019), motivation (Berridge, 2004), and neuroendocrine control (Dunn et al., 2012). Due to its widespread modulatory effects, the dopamine system remains one of the most widely researched biological systems since it was first discovered in the 1950s (Yeragani et al., 2010).

Extensive research in both animals (Brake et al., 2000; McArthur et al., 2005) and humans (Egerton et al., 2016; Pruessner et al., 2004) has shown that the dopamine system is particularly sensitive to pre- and post-natal environmental factors including malnutrition (Alamy et al., 2012; Susser et al., 2008), stress (Sinclair et al., 2014), exposure to toxic substances (Kim et al., 2021) and well as abuse and trauma (Sheu et al., 2010). Moreover, critical aspects of human cognition modulated by dopamine, such as attention, and goal-oriented behaviour change significantly during childhood, adolescence, and early adulthood (Hartley & Sommerville, 2015; Li et al., 2010).

1.1.1. Limitations in Studying the Human Dopamine System

The current understanding of the development of the dopamine system stems largely from experiments conducted with non-human animals. These studies have limited translation across species since sources of influence as well as developmental timing can vary significantly (Gatzke-Kopp, 2011). Comparatively speaking, neural development occurring in the early

postnatal period in several animal models corresponds to processes that appear to occur in humans prenatally (Clancy et al., 2001).

In humans, the gold standard for studying the dopaminergic system in-vivo is positron emission tomography (PET). This technique involves an intravenous administration of a radioligand of dopamine e.g., [^{11}C] raclopride to detect behaviour and/or pharmacologically induced changes in the synaptic concentration of dopamine. Since PET scans require radiation exposure, they are mainly used for diagnostic purposes and in clinical populations and are deemed an unsuitable tool for imaging developing brains.

These limitations regarding invasiveness and translatability have been mitigated by recent advances in Magnetic Resonance Imaging (MRI). It is now possible to non-invasively obtain direct measures of dopamine availability, using MRI, in the form of a neuromelanin sensitive contrast. This technique known as Neuromelanin Sensitive Magnetic Resonance Imaging (NM-MRI) capitalizes on the paramagnetic properties of neuromelanin, a by-product of dopamine metabolism.

1.2. Neuromelanin

Neuromelanin (NM) is a dark, insoluble neuronal pigment formed as a by-product of the metabolism of cytosolic dopamine in the human brain (Sulzer et al., 2000). Higher concentrations of NM are found primarily in the dopaminergic neurons of the substantia nigra (Zucca et al., 2004) and the noradrenergic neurons of the locus coeruleus (Ito et al., 2017). NM is also found in several distinct regions of the brain including the hypothalamus, medulla oblongata, cerebellum, and the premotor cortex (Zucca et al., 2014). Animal studies in rats (Zecca et al., 2008), frogs (Kemali & Gioffré, 1985), dogs (DeMattei et al., 1986), and monkeys (Herrero et al., 1993) have found NM containing neurons in these animals

NM is formed via a cascade of reactions beginning with the iron-dependant oxidation of excessive cytosolic dopamine and catecholamines. This oxidation results in the formation of highly reactive called quinones. Quinones can attach to aggregated proteins with β-structured configurations. This process initiates an oxidative polymerization process giving rise to eumelanin and pheomelanin (subtypes of melanin) containing compounds. Eumelanin and pheomelanin have the capacity to bind significant amounts of metals, particularly iron.

Through the process of macroautophagy, the resulting material that cannot be degraded is engulfed by autophagic vacuoles. These vacuoles subsequently fuse with lysosomes and other autophagic vacuoles containing lipid and protein components. Consequently, organelles containing a combination of NM, metals e.g., iron, lipid bodies, and a protein matrix are formed within the SN (Zecca et al., 2000; Zucca et al., 2014; Zucca et al., 2018).

Figure 1

Mechanisms for Biosynthesis of Neuromelanin in the Human Substantia Nigra

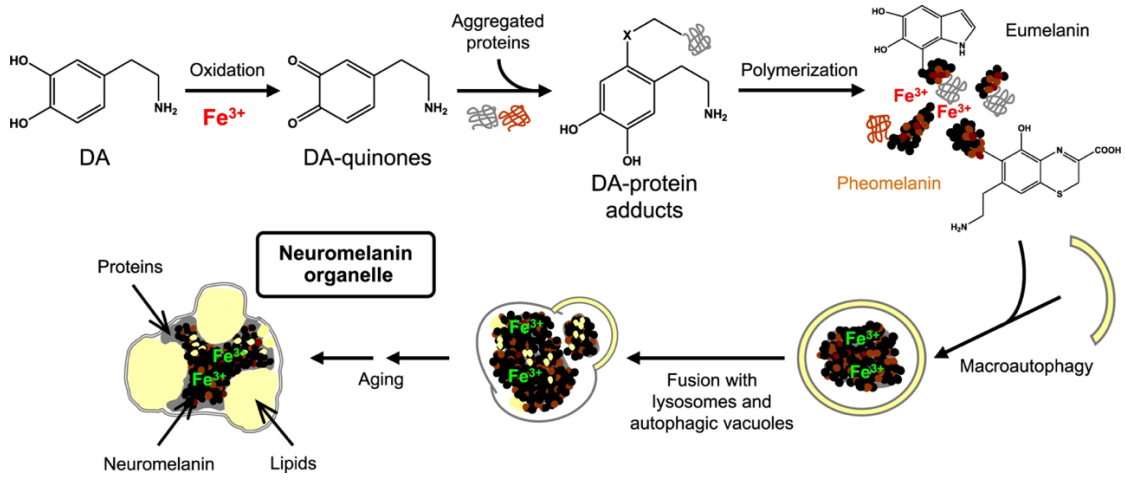

Note. Excess dopamine in the brain is prone of oxidation due to the presence of iron in dopamine rich areas of the brain such as the SN. This oxidation can lead to the creation of reactive intermediates that undergo polymerization reactions. Consequently, dopamine molecules are joined together to form larger chemical structures. The polymerization of oxidized dopamine leads to the formation of neuromelanin precursors e.g., euromelanin.

These precursors undergo the process of macroautophagy and fuse with lysosomes and autophagic vacuous. Eventually, they bind with other molecules including lipids, proteins, and metal ions to form NM-containing organelles (Sulzer et al., 2018).

1.2.1. Biological Role of Neuromelanin

Historically, NM was thought to be an inert waste product of dopamine metabolism with no function. However, research has shown a dual effect of NM as neuroprotective and neurotoxic, depending on its cellular environment. Since NM has the capacity to bind with metal ions, it can sequester excess amounts of these potentially toxic ions into vesicles preventing them from exerting cytotoxic effects. In addition, NM can serve to protect against oxidative stress caused by a lack of antioxidants and an excess of quinones and semi-quinones in catecholamine rich areas of the brain (Zecca et al., 2008). On the other hand, NM is released from dying neurons in extracellular space. The metal ions bound to NM are also released along with it. This may trigger neurodegenerative processes such as those underlying parkinsonism (Xing et al., 2018).

1.2.2. Age-related Accumulation of Neuromelanin

NM is absent at birth and first appears between the age of 2- and 3-years in the human SN (Cowen, 1986). The accumulation of NM appears to follow an inverted U-shaped pattern, increasing steadily until the age of between 40- and 50-years followed by a decline there onwards (Xing et al., 2018).

Figure 2

Changes in Contrast to Noise Ratio of NM-MRI Signal with Age

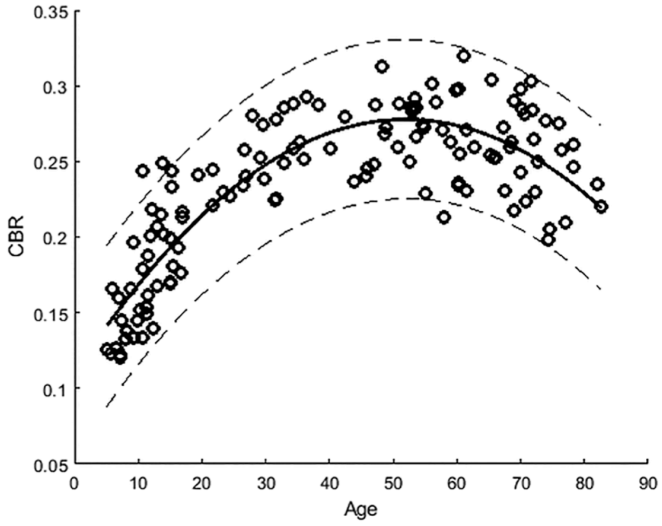

*Note.*NM accumulation follows an inverted U-shaped pattern. It increases from birth until middle age and then decreases steadily there onwards. In cases of neurodegenerative disorders e.g., Parkinsonism, the degradation of NM containing organelles (and NM-MRI signal subsequently) are much more rapid after the onset of disease (Xing et al., 2018).

1.3. Neuromelanin Sensitive Magnetic Resonance Imaging (NM-MRI)

The NM-iron complexes present in the NM organelles are paramagnetic in nature and can therefore be non-invasively visualized using a family of MRI sequences known as NM-MRI (Cassidy et al., 2019). Typically, NM-MRI is based on T1-weighted turbo spin echo (TSE) pulse sequence (Wieland et al., 2021). Initially, the shortened T1 relaxation times in NM-rich areas was thought to be responsible for the high signal in these areas (Sasaki et al., 2006). Subsequent research showed that although NM-MRI relies on T1-weighted turbo spin echo (TSE) sequences,

these sequences can be influenced by unintended magnetization transfer (MT) effects due to the extended train of refocusing pulses in multi slice image acquisitions (Trujillo et al., 2017). Indeed, MT pulse preparation of NM-MRI signal yields a higher contrast even at low field strength MRI (e.g., 1.5T; Nakane et al., 2008)

While other methods for studying dopamine in vivo exist, NM-MRI has attracted the attention of researchers for its ability to non-invasively image the brain. Since this technique doesn't require radiation exposure, it is safe for use in developing populations.

1.3.1. NM-MRI: A Non-Invasive Proxy Measure for Dopamine Functioning

Cassidy and colleagues (2019) demonstrated NM-MRI as a non-invasive proxy measure for dopamine functioning the human brain. They conducted a series of analysis comparing NM-MRI with pre-established techniques for imaging the dopamine system. A significant positive correlation was found between the quantity of NM measured by NM-MRI and other imaging modalities i.e., PET and functional MRI. In addition, Cassidy and colleagues (2019) conducted histological analyses of post-mortem brain tissues in the substantia nigra to quantitatively assess the presence of NM. These brain specimens were later imaged with a NM sensitive contrast. A strong positive correlation was found between estimates of neuromelanin quantified via histological and NM-MRI.

1.3.2. Utility of NM-MRI for Neuropsychiatric Research

Several studies have also established the utility of NM-MRI for capture meaningful differences in midbrain and striatal dopamine levels amongst those with Parkinson's disease

(Matsuura et al., 2013; Ohtsuka et al., 2014) and schizophrenia (Horga et al., 2021; Ueno et al., 2022), disorders characterized by a substantial decrease and increase in dopamine levels respectively. Not only has the technique proven useful for discriminating between individuals with Parkinson's Disease from those without it, Cassidy and colleagues (2019) found that NM-MRI signal can capture biologically meaningful variation across anatomical subregions within the substantia nigra. Moreover, NM-MRI was also able to replicate the known anatomical topography of dopamine neuron loss within the substantia nigra.

NM-MRI has also been studied in the context of cocaine dependence. Cassidy and colleagues (2020) found NM-MRI to be a reliable measure for distinguishing between those with a history of cocaine use and age/sex-matched controls. A significant increase in NM-MRI signal was found in those with a cocaine dependence disorder.

Together, these studies substantiate NM-MRI as a reliable and valid measure of studying dopamine functioning in vivo.

1.4. Quantifying NM-MRI Signal

NM-MRI signal can be quantified in the form of a Contrast to Noise Ratio (CNR)—the relative difference in signal intensity between an area containing neuromelanin organelles and surrounding white matter (Salzman et al., 2021). A higher NM-MRI CNR has been found in areas known to contain neuromelanin, such as the SN (Chen et al., 2014) or the LC (Langley et al., 2017). On the other hand, a low NM-MRI CNR is found in regions known to have little to no neuromelanin e.g., cerebral peduncle (Wang et al., 2021), brain stem (Xing et al., 2022), and crus cerebri (Cassidy et al., 2020; Ueno et al., 2022; Wengler et al., 2020). Calculating CNR for quantifying NM-MRI signal has been extensively studied and validated across different age

groups (Al Haddad et al., 2023; Xing et al., 2018) and diagnostic categories (Isias et al., 2016; Wengler et al., 2021; Ueno et al., 2022).

1.4.1. Atlas-based Segmentation Approach

One approach to identifying a region of interest (ROI) and a background/reference region is atlas-based segmentation. Atlas-based segmentation involves utilizing a pre-segmented reference image (atlas) and transforming its segmentation onto a new target image through image registration. This process of image registration helps reduce variations in brain anatomy and positioning between the atlas and the target image by calculating a deformation field. The deformation field contains information regarding how each voxel in the atlas image should be transformed to align with the target image and remove differences in neuroanatomy between the two images.

1.4.1.1. Advantages of the Atlas-based Segmentation

Ease of Access. Atlases are readily available and can be time and cost-efficient since they drastically reduce manual labour costs.

Voxel wise Analysis of Contrast to Noise Ratio. Standardized atlases can be used to perform a voxel wise analysis of CNR. The normalization of both a participant's brain image and an atlas in the same space allows us to achieve accurate registration between subjects across all voxels contained within a brain region and across brain regions. A voxel wise analysis is useful for a detailed investigation of the topographical patterns and tissue characterization in different regions of the brain and/or within a specific brain area (Cassidy et al., 2019). Voxel wise analyses can be used to combine data from multiple subjects and investigate population-level effects. This helps identify consistent patterns of activity or differences across subjects. Conversely, a voxel-wise analysis enables whole-brain exploration without requiring a priori

assumptions about specific regions of interest, thereby revealing unexpected activations or interactions.

1.4.1.2. Limitations of Atlas-based Segmentation

Anatomical variability. Since the atlases are created from a sample different than that it is used for, anatomical variations among different individuals can lead to challenges in accurately registering the atlas to the target image leading to inaccurate segmentations (Rao et al., 2017). Atlas-based segmentations have a low accuracy when defining boundaries in small regions This can be problematic especially in cases of overlapping anatomical structures.

Utility for brain images from patient populations. Moreover, atlas-based approaches struggle significantly in cases of neuropathology whereby idiosyncratic changes in brain tissue and structures can affect image alignment and segmentation accuracy.

1.4.2. Manual Segmentation Approach

Manual segmentation of ROIs is a fundamental, gold standard technique used in MRI image processing to delineate specific structures and areas within images. This process involves a trained human expert in neuroanatomy (e.g., neuroradiologist) to carefully draw the boundaries around the desired regions for each participant individually using specialized software.

1.4.2.1. Advantages of Manual Segmentation

High Accuracy and Validity. Manual segmentation technique arguably provides the most accurate characterization of neuronal tissue and localization of specific structures within an image (Magadza & Viriri, 2021). This is a fundamental step for measuring volumes, tracking changes over time, and studying relationships e.g., connectivity pattern between structural and/or functionally distinct brain areas.

Anatomical Specificity. Manual segmentation approaches have higher levels of specificity and sensitivity than automated approaches, especially when small brain structures are being investigated. Often these approaches can serve as a ground truth against which the performance of automated segmentation algorithms is evaluated.

1.4.2.2. Limitations of Manual Segmentations

Time-Consuming and Labor-Intensive. Manual segmentations require a human expert and are therefore quite costly. In addition, the process of manual delineating complex brain structures with sufficient accuracy can be a laborious endeavour.

1.5. Ultra-High Field Strength Neuromelanin Imaging

NM-MRI experiments have primarily been conducted at a 3 Tesla (3T) MRI field strength. The choice of MRI field strength can influence the quality of neuromelanin imaging. Neuromelanin has subtle contrast characteristics and achieving a high spatial resolution in NM-MRI can be challenging because neuromelanin production nuclei e.g., substantia nigra (SN) and locus coeruleus (LC) are significantly small and therefore harder to image and localize. This explains the dearth of research probing the impact of development on midbrain nuclei, the actual sites for dopamine production. Indeed, several studies in the past have investigated developmentally meaningful changes in the dopamine system by examining physically larger areas of the brain e.g., the striatum (Tang et al., 2001) and the prefrontal cortex (Del Arco & Mora, 2008; Garris et al., 1993).

Higher resolution is necessary to accurately differentiate and visualize NM from surrounding tissues. This can be achieved through ultra-high field strength imaging, such as by employing 7 Tesla (7T) MRI scanning. High field strength scanner can potentially enhance the contrast between neuromelanin-containing areas (e.g., the SN) and other brain structures thereby

improving sensitivity and specificity to NM-MRI imaging. Hence, NM-MRI images generated from a high-field strength MRI scanner bear the promise of providing a unique opportunity for studying the functional and anatomical organization of midbrain dopaminergic nuclei with enhanced cortical detail, reduced blurring between gray and white matter and a significantly higher signal to noise ratio (Kerchner, 2011).

While 7T MRI has several advantages over 3T, it is not without its limitations. Some challenges associated with 7T MRI include increased susceptibility to artifacts caused by magnetic field inhomogeneities and longer scan times due to higher resolution imaging. In additional, the significant differences in contrast and anatomical detail between 3T and 7T makes it challenging to accurately compare MRI data acquired from the two field strengths. Hence, before we can harness the benefits of ultra-high field strength NM-MRI imaging, it is critical to determine whether the statistical techniques and neuroimaging processing used for segmenting, quantifying, and analyzing neuromelanin-containing regions at 3T transfer reliably to 7T NM-MRI. In this case, a higher convergence between the two field strengths would make us relatively confident that the molecular quantification from the sequences reliably generate the same estimates of NM.

Figure 3

NM-MRI iImages Acquired from the Same Person at Both 7T and 3T

A 

B 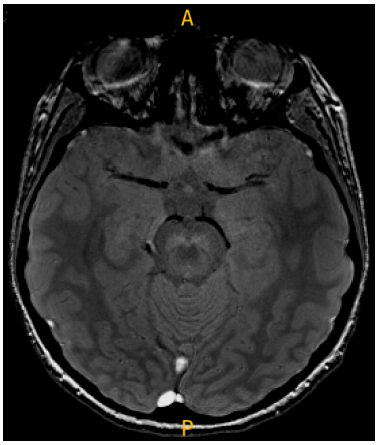

Note. (A) NM-MRI images acquired at 7T & (B) NM-MRI images acquired at 3T. The cortical detail and contrast are significantly increased in the (A) compared to (B). Slice is clearly showing the midbrain. The SN has a better tissue contrast in 7T vs 3T.

1.6. Research Objective and Hypothesis

The purpose of this study, therefore, is to determine whether estimates of NM content obtained from 3T NM-MRI images reliably converge with those acquired using 7T NM-MRI scans. We hypothesize that there would be strong positive correlation between contrast to noise ratio (CNR) based estimates of NM sensitive signal 3T and 7T. Moreover, we expect a higher CNR value at 7T as opposed to 3T for each participant due to the enhanced spatial resolution and contrast quality characteristic of high field strength imaging.

2. Methods

2.1. Participants

A community sample consisting of 28 healthy adult participants between the ages of 19-73 years (mean age = 45.5 yrs., # of females = 16) was recruited from London, Ontario.

Participants were recruited via advertisement postered by the Centre for Functional Metabolic Mapping for voluntary participation in a structural imaging study. The dataset was commissioned by Biogen, a technological firm in Boston, USA with provisions made for scientific and research purposes. Inclusion criteria were age over 18 years, no MRI contraindications, and no history of psychiatric and/or neurological disorders. All procedures were approved by Western University's Ethics Review Board. Written informed consent was acquired from each participant.

Figure 4

Illustration of the Research Design of the Current Study

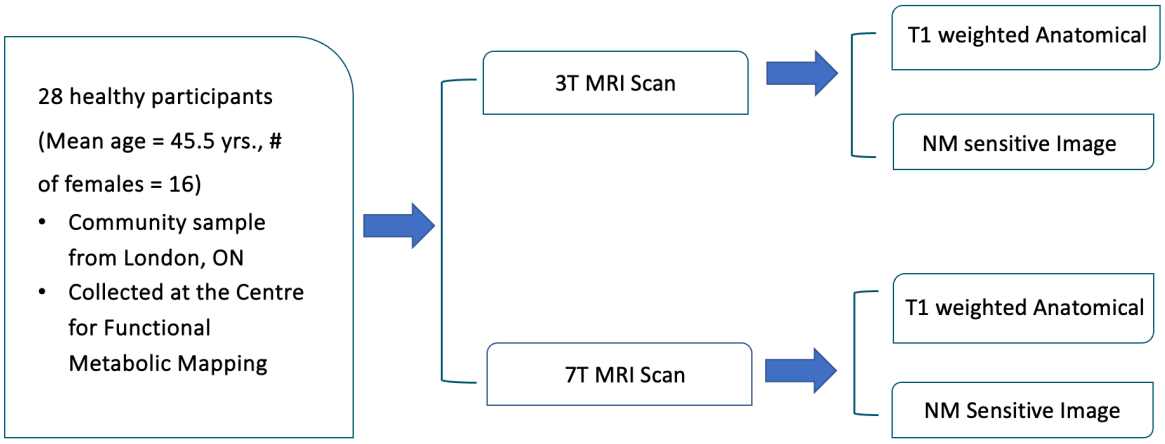

2.2. Magnetic Resonance Imaging Acquisition Protocol

Whole-brain 3D anatomical (T1-MPRAGE), and NM-sensitive 3D multi-echo GRE volumes were obtained from all participants at both 3T and 7T field strengths, using Siemens MAGNETOM 3T Prisma Fit with a 32-Channel Head Coil and Siemens MAGNETOM 7T MRI Plus 32-Channel Head Coil scanners respectively. This research design provided the opportunity to conduct a within-subject estimation of NM content across the two field strengths and directly compare the convergence in NM estimations.

Figure 5

Age Distribution of the Sample

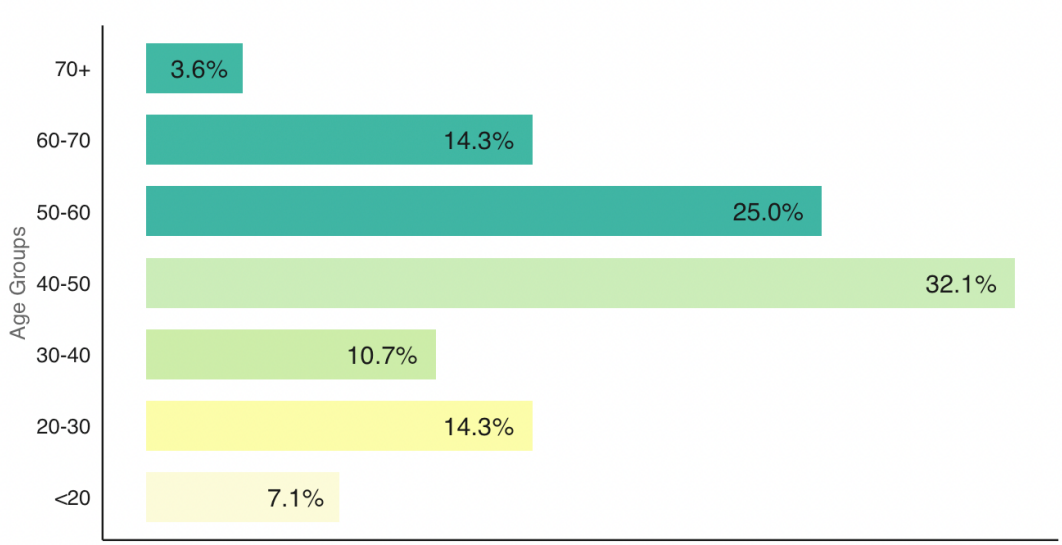

2.2.1 Image Acquisition at 3-Tesla

2.2.1.1. Anatomical Acquisition

T1-weighted (T1w) image was acquired at 3T for processing the NM-MRI images with the following parameters: spatial resolution = 1x1x1 mm^3; repetition time (TR) = 2300 ms; inversion time (TI) = 900 ms; flip angle = 9°; echo time (TE) = 2.98 ms; field-of-view (FOV) = 240 x 256 x176 mm^3; Number of slices = 176; in-plane acceleration, GRAPPA = 2; bandwidth = 210 Hz/pixel.

2.2.1.2. NM-MRI Acquisition

The parameters for 3D multi-echo GRE volumes obtained at 3T were set as follows: spatial resolution = 0.60 x 0.60 x 1.5 mm^3; TR = 54 ms; flip angle = 16°; TE = 23.54 ms; FOV = 263 x 350 x 350 mm^3; in-plane acceleration, GRAPPA = 2; slice thickness; 1.5 mm; number of slices = 36; bandwidth = 130 Hz/pixel.

2.2.2. Image Acquisition at 7-Tesla

2.2.2.1. Anatomical Acquisition

The parameters for the T1w image acquired at 7T were as follows: spatial resolution = 0.70 x 0.7 x 0.7 mm^3; TR = 6000 ms; TI = 2700 ms; flip angle = 4°; TE = 2.70 ms; FOV = 220 x 220 x 146 mm^3; in-plane acceleration, GRAPPA = 3; bandwidth = 140 Hz/pixel.

2.2.2.2. NM-MRI Acquisition

NM MRI images collected using the 7T MRI scan had the following parameters: spatial resolution = 0.40 x 0.40 x 1.0 mm^3; TR = 75 ms; flip angle = 8°; TE = 8.80 ms; FOV = 144 x 192 x 52 mm^3; in-plane acceleration, GRAPPA = 2; slice thickness; 1 mm; number of slices = 53; bandwidth = 250 Hz/pixel.

2.2.3. NM Image Quality Control

Quality control checks were performed according to the procedures outlined by Salzman and Colleagues (2021). Briefly speaking, all images were visually inspected for motion artifacts, abrupt shifts in signal intensity exhibiting a linear pattern that disregards typical anatomical boundaries, and sufficient coverage of the ROIs (SN and CC).

3. Data Analysis and Results

NM content was not related to participants' age or sex at either 3T or 7T. This was true across both atlas-based and manually segmentation methods.

3.1. Atlas-based Segmentation Method

All analyses were conducted in the native space of the participant using MATLAB scripts. We obtained template masks of SN and CC used in Cassidy and colleagues (2019) from the researcher to identify voxels corresponding to the ROI and the background respectively.

These masks were created in MNI space by manual tracing of the CC and SN on a composite NM-MRI image (created by averaging MNI NM-MRI scans of 40 healthy individuals). SN and CC masks were inverse transformed into the native space of all participants at both 3T and 7T.

This procedure was conducted using Statistical Parametric Mapping Software (SPM-12) within MATLAB. First, we co-registered each participant's NM image with their T1w scan. The co-registered T1w image was then segmented using SPM-12's tissue probability masks. Inverse and forward deformation fields were calculated at the segmentation step. The inverse deformation field describes how the atlas image needs to be deformed to match the anatomy of the participant. The calculated inverse transformation was applied to both the CC and SN masks. This process warped the segmented atlas from the common stereotaxic space back to the subject's image space. This process was done for each participant at both 3T and 7T.

Figure 6

NM-MRI scan at 3T showing the Substantia Nigra and the Crus Cerebri

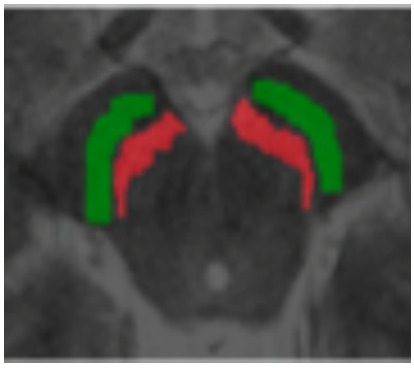

Note. The substantia nigra, highlighted in red appears as a hyperintense (lighter) region on NM-MRI scan while the crus cerebri, highlighted in green is hypointense i.e., darker and has less contrast.

3.1.1. Data Analysis: Atlas-based Segmentation

Participants' 3T and 7T images were masked using their respective SN and CC atlases to identify voxels contained within these regions. CNR in the SN was calculated as:

$$CNR_{ROI} = \frac{SI_{Substantia\ Nigra} - SI_{Crus\ Cerebri}}{SI_{Crus\ Cerebri}}$$

where $SI_{Substantia\ Nigra}$ is the mean signal intensity within SN voxels and $SI_{Crus\ Cerebri}$ is the mean signal intensity of all voxels within the crus cerebri, a region adjacent to the SN with little to no neuromelanin.

This equation for calculating CNR has been extensively used in NM-MRI research (Ohtsuka et al., 2018, van der Pluijm and collegues 2021; Wang et al., 2021; Xing et al., 2018).

3.1.2. Results: Atlas-based Segmentation

A box plot was created from the CNR values to identify potential outliers. Values considered outliers (n = 4) and eliminated from further statistical analyses.

We computed a Spearman's rank correlation coefficient to assess the statistical dependence between the ranking of participant CNR values at 3T and 7T. We found a small negative correlation between the two variables that failed to reach significance, $r(22) = -.14$, $p = .50$, Mean $CNR_{3T} = 0.51$; $CNR_{7T} = 0.74$

Figure 7

Relationship Between Mean CNR for NM-MRI signal at 3T with that at 7T

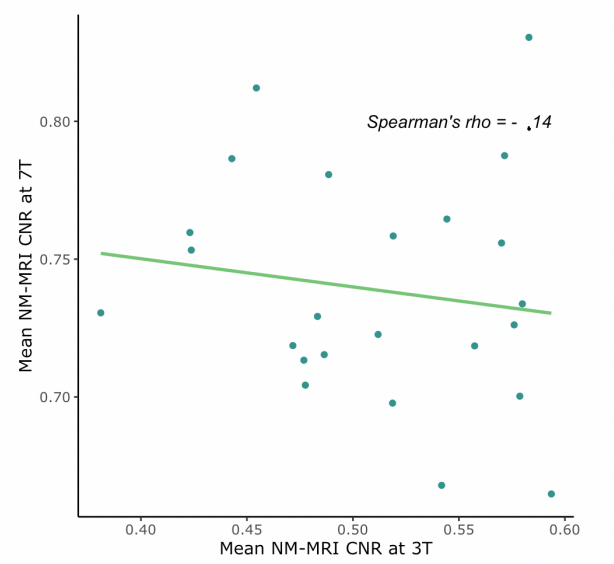

Note. A small non-significant correlation was found; Spearman's rho: -.14, p = .50

The CNR values obtained with the atlas-based segmentation were unexpected since the same participant provided data at both 3T and 7T. Therefore, we expected the rank ordering of participants with respect to their CNR values to remain consistent between the two field strengths. Upon visual inspection in ITK-SNAP, it became clear that the inverse transformed atlases were not accurately overlaid on the SN for participant. The mask seemed to lack specificity and was observed to be encroaching on what is considered the CC.

Figure 8

Atlas-based Segmentation at 3T

A

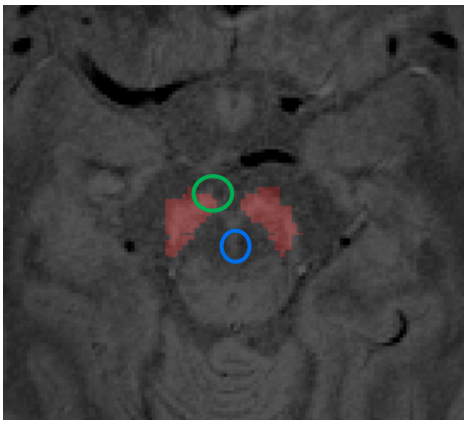

B

Note. (A) Overlay of inverse transformed SN atlas, shown in red, on top of the participant's anatomy. Green circle highlights voxels of the crus cerebri (lower intensity, no neuromelanin) erroneous identified by the atlas as SN, demonstrating a lack of specificity. Blue circle corresponds to SN voxels that were omitted by the atlas, demonstrating a lack of sensitivity of the atlas as a template mask. (B) NM-MRI image showing the midbrain of the participant without the atlas overlaid.

Figure 9

Atlas-based Segmentation at 7T

A

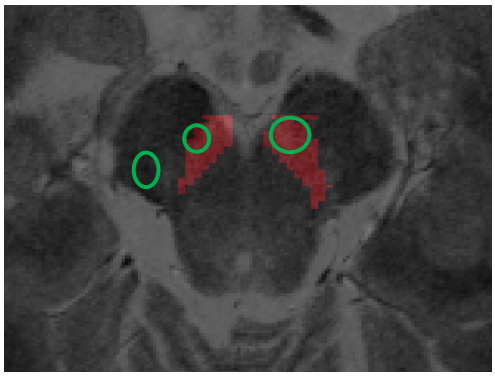

B

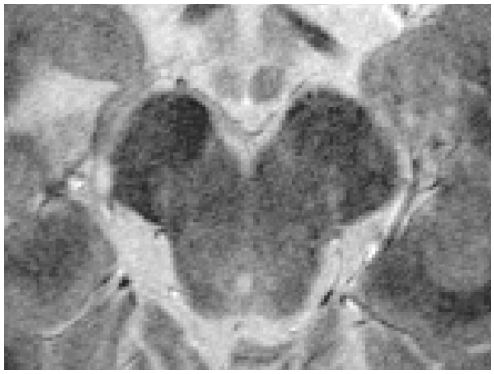

Note. (A) Overlay of inverse transformed SN atlas, shown in red, on top of the participant's anatomy. Green circle highlights voxels of the crus cerebri erroneous identified by the atlas as SN, demonstrating a lack of specificity. (B) NM-MRI image showing the midbrain of the participant without the atlas overlaid.

3.2. Manual Segmentation

As an alternative, to the atlas-based segmentation approach, we obtained manually segmented masks of the SN for each participant individually. To this end, the SN in the NM images was manually segmented by a trained neuroradiologist (L.H.) for each NM-MRI image for 25 participants using ITK-SNAP (v3.8.0) at 3T & 7T. Each binarized manually segmented drawing of the SN were used to identify SN voxels within its corresponding NM-MRI image. These segmentations allowed us to conduct a region of interest (ROI) based analysis of CNR in the native space of the participant.

Background distribution was defined by the crus cerebri. To identify voxels corresponding to the crus cerebri, we inverse transformed the crus cerebri mask obtained from Cassidy and colleagues (2019) into the native space of each participant. This was achieved using SPM-12. We applied the inverse transformation matrix acquired during the normalization of NM-MRI image for each participant to the normalized crus cerebri image.

Figure 10

Manual Segmentation at 3T

A

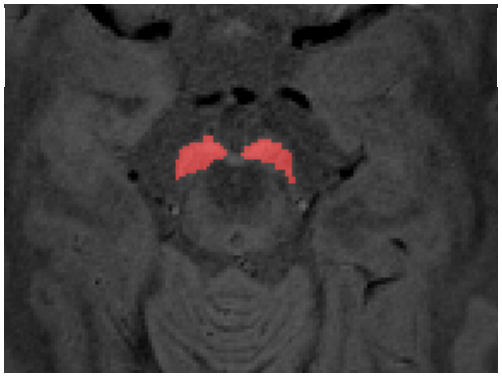

B

Note. (A) Shows manual segmented mask at 3T created by a neuroradiologist overlaid on its corresponding image. Compared to the inverse transformed atlas, the manually segmented masks have a higher sensitivity and specificity. (B) NM-MRI image showing the midbrain of the participant without the atlas overlaid.

Figure 11

Manual Segmentation at 7T

A

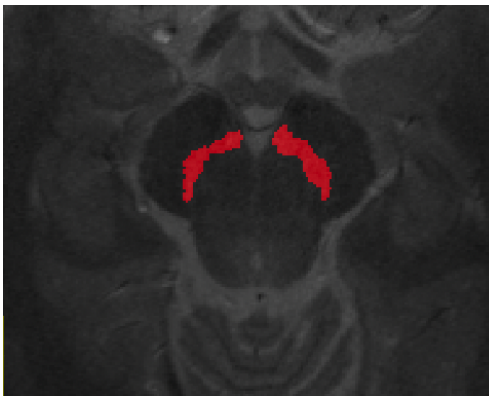

B

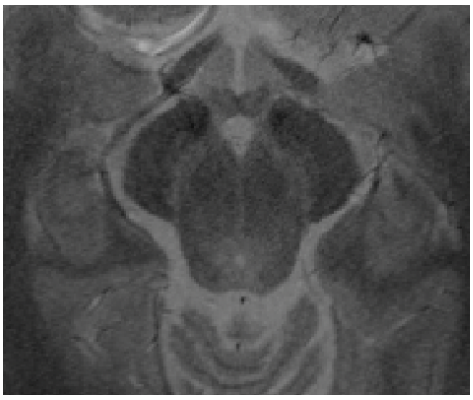

Note. (A) Shows manual segmented mask at 7T created by a neuroradiologist overlaid on its corresponding image. Compared to the inverse transformed atlas, the manually segmented masks have a higher sensitivity and specificity. (B) NM-MRI image showing the midbrain of the participant without the atlas overlaid.

3.2.1. Data Analysis: Manual Segmentation

CNR values were calculated using a custom MATLAB script. To obtain CNR estimates, for each participant, we subtracted the mean signal intensity (SI) within all voxels corresponding to SN from the mean signal intensity within voxels corresponding to the crus cerebri. The result was then divided by the background intensity (i.e., mean signal intensity in the crus cerebri) as:

$$CNR_{ROI} = \frac{SI_{Substantia\ Nigra} - SI_{Crus\ Cerebri}}{SI_{Crus\ Cerebri}}$$

This process was done for both 3T and 7T images for each participant.

3.2.2. Results: Manual Segmentation

To identify and eliminate potential outliers. CNR values were transformed into z-scores. Values greater than 3.5 or less than -3.5 were considered outliers (n = 2) and eliminated from further statistical analyses.

We computed a Spearman's rank correlation coefficient to assess the relationship between CNR values at 3T and 7T. We found a modest positive correlation between the two variables that failed to reach significance, $r(21) = .42$, $p = .05$, Mean $CNR_{3T} = 0.0621$; $CNR_{7T} = 0.071$

Figure 12

Relationship between Mean NM-MRI CNR at 3T and 7T Using Manual Segmentation

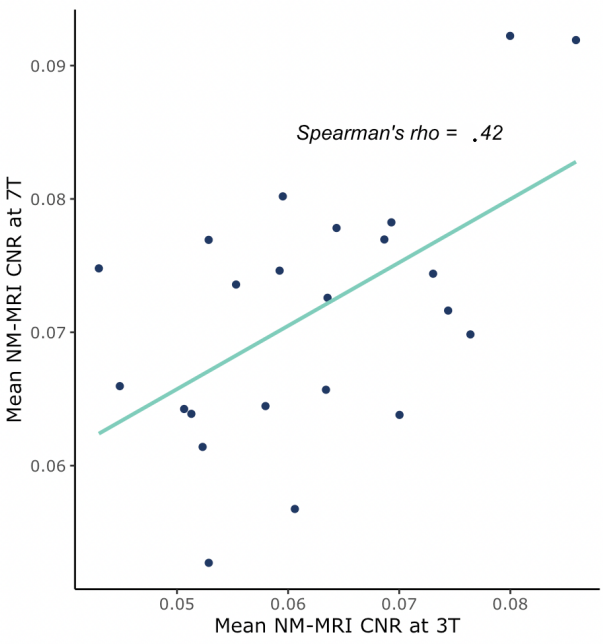

Note. A modest positive correlation was found; Spearman's rho = .42; p = .05

4. Exploratory Analyses

Given that the comparison was conducted with data acquired from the same participant at both 3T and 7T, an only modest correlation was surprising. Hence, we conducted some exploratory analyses to further investigate the results we obtained.

4.1. Boundary Drawing of Manually Segmentations

A potential reason for the modest correlation observed pertains to the differences in the way the boundaries of the SN were drawn for 3T vs 7T images by the neuroradiologist. To investigate this possibility, a fellow graduate student in our lab, Aria Fallah conducted exploratory analyses by comparing the volume of SN across 3T and 7T using the manually segmented images.

For each participant, the total number of voxels within the ROI i.e., SN were multiplied by voxel dimensions of the image to obtain final volume estimates at both 3T and 7T.

Similar to the results for the CNR values, only a modest correlation was found between 3T and 7T volumes: $r_s(23) = .490$, $p = .012$. This finding lends support to the explanation for our CNR estimates.

Figure 13

Relationship Between Substantia Nigra Volumes in (mm^3) at 3T and 7T

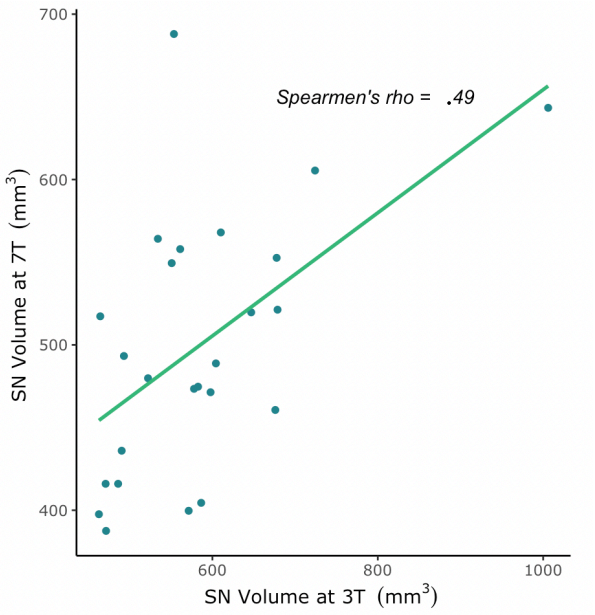

Note. Volumes at 3T and 7T were only moderately correlated; Spearman's rho = .49, p = .01. Image created from data published in Fallah, 2023. Data was used with permission from the author.

4.2. Same Mask for 3T and 7T NM-MRI Images

To potentially mitigate the effect of differences in boundary drawings for manually segmented atlases, we sought to co-register 7T images (NM and manually segmented atlas) with the 3T images, using SPM-12. This process, however, was only partially successful. We were able to co-register a subset of participant NM images (n = 20). However, because of the the lack

of sufficient anatomical landmarks within the binarized atlases, SPM-12 did not have nearly enough information to successful execute the co-registration procedure. As an alternative, we used a participant's manually segmented atlas at 3T to mask both 7T and 3T images and identify the voxels within the SN. Using the same mask partially circumvented the problem of differences in SN volumes between the two field strengths. CNR was calculated as described above.

A boxplot was created with the CNR values to identify potential outliers. In addition, CNR values were transformed into z-scores. Values greater than 3.5 or less than -3.5 were considered outliers (n = 1) and eliminated from further statistical analyses.

A non-significant small Spearman's rank correlation was found between CNR at 3T and 7T using this method: $r(17) = .303$, $p = .20$, Mean $CNR_{3T} = 0.196$; $CNR_{7T} = 0.164$

Figure 14

Relationship Between Mean NM-MRI CNR at 3T and 7T Calculated Using Manually Segmented Substantia Nigra Mask at 3T

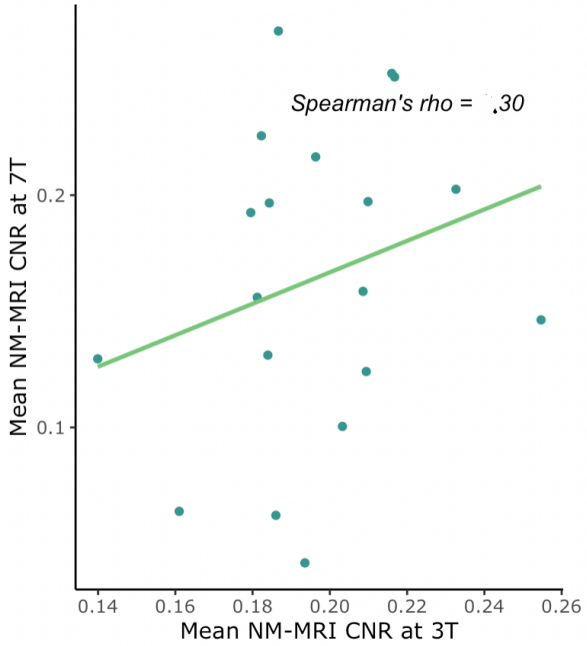

Note. Non-significant small convergence was found between 3T and 7T; Spearman's rho= .3, p = .20

4.3. Other Mathematical Equations for CNR

4.3.1. Standard Deviation of Background as Noise

In the NM-MRI literature, another method for calculating CNR consists of using the Standard deviation of the background region as the denominator (Isaias et al., 2016; Lee et al., 2021; Wang et al., 2018). This provides a measure how spread out the values in the background distribution are around the mean.

4.3.1.1. Manually Segmented Images

We applied the following formula of calculating CNR from the NM-MRI images co-registered 3T and 7T images (as described in 3.3.2.). This analysis allowed us to examine in difference in CNR values as a function of the model used for calculation.

$$CNR_{ROI} = \frac{Mean\ SI_{Substantia\ Nigra} - Mean\ SI_{Crus\ Cerebri}}{Standard\ Deviation\ of\ SI_{Crus\ Cerebri}}$$

A boxplot was created with the CNR values to identify potential outliers. In addition, CNR values were transformed into z-scores. No outliers were found.

The CNR at 3T and 7T was strongly associated, $r(18) = .791$, $p < .001$, Mean CNR_{3T} = 3.99; CNR_{7T} = 1.34

Figure 15

Relationship Between Mean NM-MRI CNR at 3T and 7T Calculated Using the Standard Deviation of Crus Cerebri to Define Background Noise on Manually Segmented Images

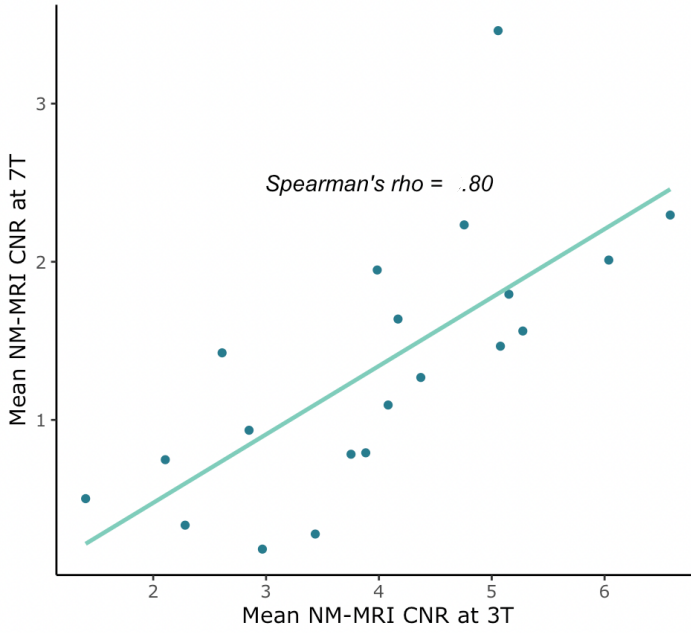

Note. Significant large correlation was found between 3T and 7T; Spearman's rho= .80, $p < .001$. Analyses were conducted on data from manually images segmented images co-registered to 3T native space of the participant

4.3.1.2. Images Segmented Using an Atlas

We repeated the analysis outlined in 4.3.1.1. using images segmented via the Cassidy Atlas to investigate if the atlas-based approach also yields different CNR values as a function of the model used for calculation.

CNR values were calculated using the equation in 4.3.1.1. as:

$$CNR_{ROI} = \frac{Mean\ SI_{Substantia\ Nigra} - Mean\ SI_{Crus\ Cerebri}}{Standard\ Deviation\ of\ SI_{Crus\ Cerebri}}$$

CNR values were plotted in the form of a boxplot to identify potential outliers. No outliers were found. CNR at 3T and 7T were strongly associated, $r(18) = .761$, $p < .001$, Mean $CNR_{3T} = 10.523$; $CNR_{7T} = 3.983$

Figure 16

Relationship Between Mean NM-MRI CNR at 3T and 7T Calculated Using the Standard Deviation of Crus Cerebri to Define Background Noise on Images Segmented Using a Standard Atlas

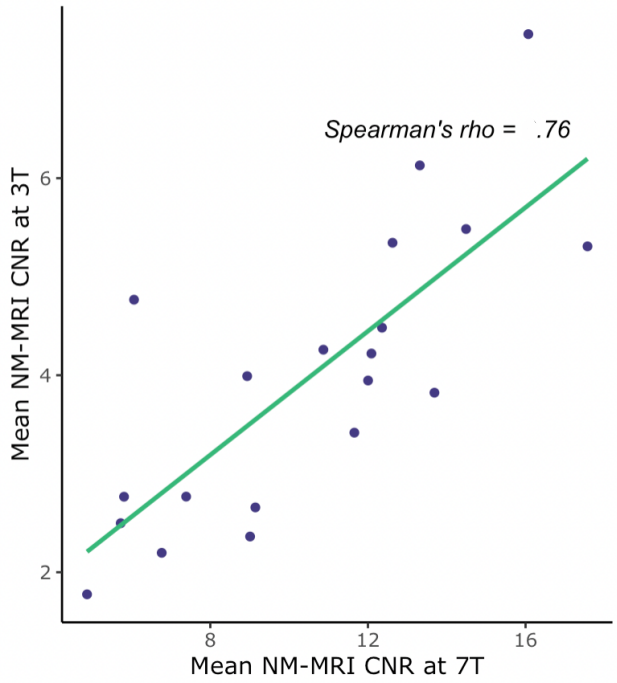

Note. Significant large correlation was found between 3T and 7T; Spearman's rho= .76, $p < .001$. Analyses were conducted on data from images segmented using the Cassidy atlas.

4.3.2. Square Root of Standard Deviations as Noise

Another model for calculating CNR is described by Partridge and colleagues (2011) in the context of Diffusion weighted MR imaging whereby the mean of signal intensity of the ROI with contrast is subtracted from a background ratio and the result is divided by the square root of the sum of standard deviation of the contrast region and the background region.

We adapted the formula described in their research for calculating NM-MRI CNR as follows:

$$CNR = \frac{Mean\ SI_{SN} - Mean\ SI_{CC}}{\sqrt{SD_{CC} + SD_{SN}}}$$

Where SI_{SN} and SI_{CC} correspond to the mean signal intensity within the Substantia Nigra and Crus Cerebri respectively. SD_{CC} and SD_{SN} denote the standard deviations of Substantia Nigra and Crus Cerebri. This formula was applied to the co-registered 3T and 7T NM-MRI images.

A boxplot was created with the CNR values 2 data points were identified as outliers. CNR at 3T and 7T were moderately associated, $r(18) = .515$, $p = .02$, Mean $CNR_{3T} = 7.86$; $CNR_{7T} = 4.62$.

Figure 17

Relationship Between Mean NM-MRI CNR at 3T And 7T Calculated Using the Square Root of Standard Deviations to Define Background Noise

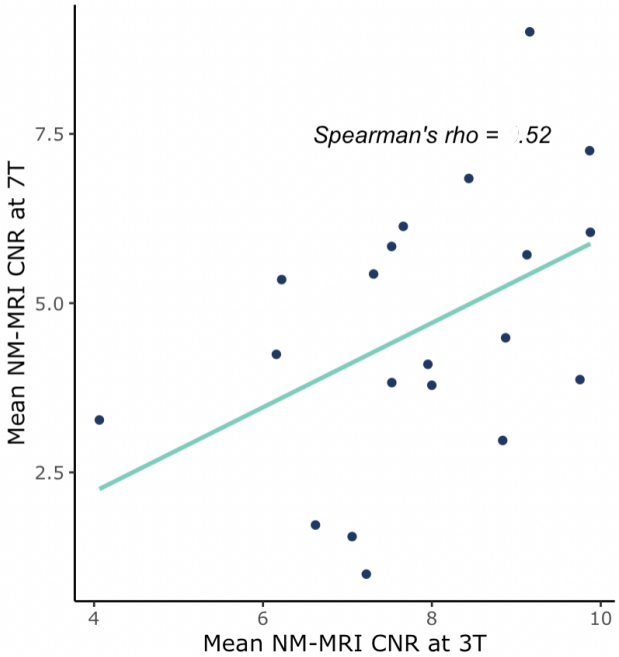

Note. Significant medium correlation was found between 3T and 7T; Spearman's rho= .5, $p = .02$

4.4. NM-MRI Signal Quantification Without a Background Region

Despite its accuracy and benefits, manually segmented drawings of atlases can be an expensive, time consuming, and labour-intensive process, as it relies on the expertise of the person performing the segmentation. Therefore, researchers are increasingly trying to find alternative methods for reliably obtaining measures of CNR. In some cases, a combination of manual and automated methods may be used to enhance efficiency and accuracy while minimizing human effort.

In our analyses, although the SN masks were manually segmented by the neuroradiologists, the background intensity was still being defined using an atlas obtained from Cassidy and colleagues (2019). This atlas of the CC was developed by obtaining an average of manually segmented drawing from a set of NM-MRI drawings (n = 40) acquired at 3T. Consequently, the inverse transformed CC masks have lower levels of specificity for capturing CC voxels than their manually segmented SN counterparts.

Here, we tried two approaches to calculating CNR that do not require a binarized mask for generating a background intensity distribution.

4.4.1. Root Mean Square Contrast

The root mean square contrast (RMS contrast) is a measure used to quantify the variation in pixel intensity within an image. It provides insight into the overall level of contrast and variability present in the image.

Here, we used the RMS contrast method to estimate CNR by computing a ratio of the overall contrast within the ROI and that within the rest of the image.

$$CNR_{RMS} = \frac{Root\ Mean\ Square\ SI_{Substantia\ Nigra}}{Root\ Mean\ Square\ SI_{Rest\ of\ the\ image}}$$

A significant medium to large Spearman's correlation was found between CNR at 3T and 7T using this method $r(21) = .70$, $p < .001$, Mean $CNR_{3T} = 1.862$; $CNR_{7T} = 1.332$

Figure 18

Relationship Between Mean NM-MRI CNR at 3T And 7T Calculated Using the Root Mean Square Method

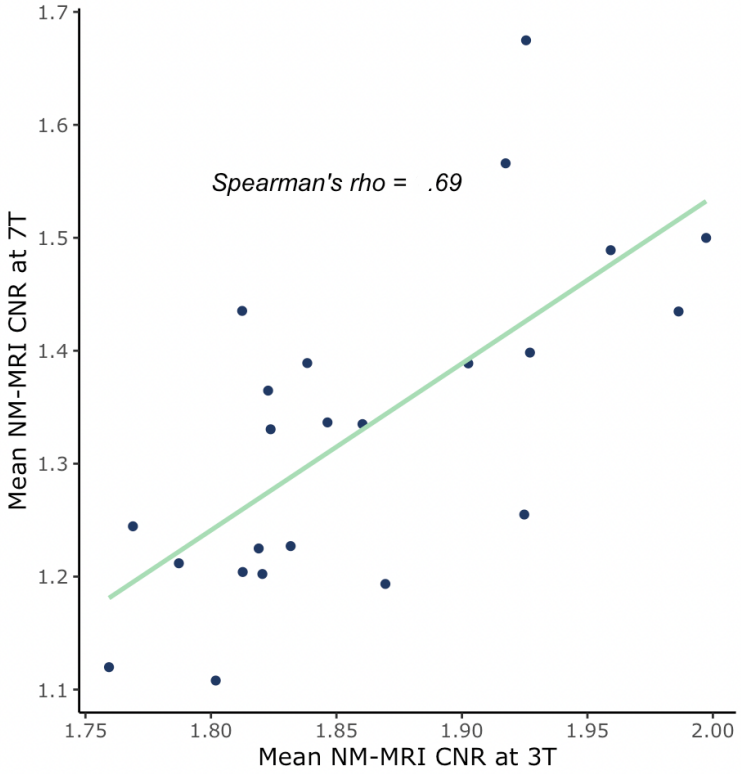

Note. Significant medium to large correlation was found between 3T and 7T; Spearman's rho= .70, $p < .001$

4.4.2. Signal to Noise Ratio

CNR is a measure that considers the contrast between different regions of interest in an image while accounting for the noise level. However, when a background region can't be

delineated, a simple signal to noise ratio can be computed. SNR is a ratio of the signal strength to the noise level in the data. It focuses on the overall quality of the signal and how well it stands out from the noise.

Signal to noise ratio was calculated as:

$$SNR = \frac{Mean\ SI_{Substantia\ Nigra}}{Standard\ Deviation\ of\ SI_{Rest\ of\ the\ image}}$$

A boxplot was created with the CNR values. In addition, CNR values were transformed into z-scores to identify potential outliers (n = 1)

CNR values at 3T and those at 7T were moderately associated, $r(17) = .47$, $p = .04$, Mean CNR_{3T} =2.667 ; CNR_{7T} = 2.189

Figure 19

Correlation Between Mean NM-MRI CNR At 3T and 7T Obtained by Calculating Signal to Noise Ratio

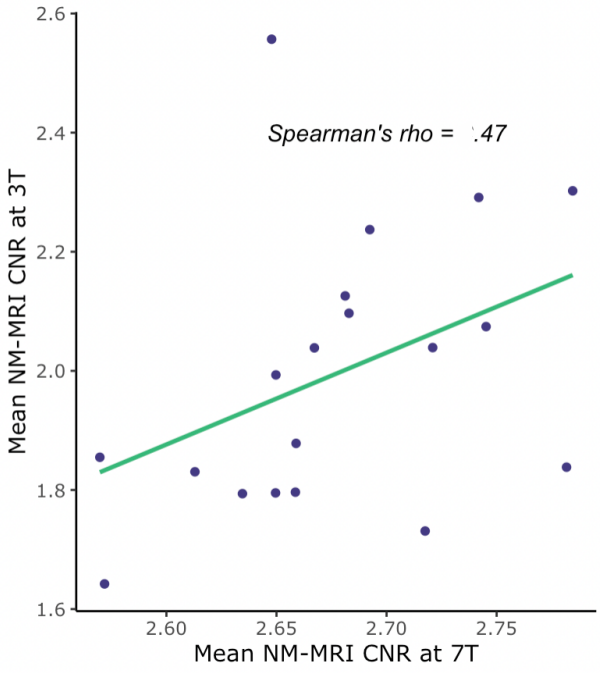

Note. Significant small to medium correlation was found r= .47, p= .04

5. Discussion

NM-MRI imaging is a growing field with applications for both applied and basic research. Advancements in MRI including a higher spatial resolution, increased contrast to noise ratio, enable us to non-invasively image the brain with enhanced sensitivity to its structural, functional, and metabolic facets. To this end, our ability to capitalize on the advantages of these advancements for NM-MRI research has been limited. Without evidence regarding the validity to molecular volumetric quantification of NM rich areas, we cannot be confident in the estimates obtained using advanced high field strength MRI. The objective of the current research study is to determine if estimates of NM-MRI signal at 3T reliably predict those obtained at 7T. We utilized the two most commonly used image segmentation approaches for this purpose. Moreover, we also conducted several exploratory analyses to gain a more comprehensive understanding of our findings.

We found that estimates of NM-MRI signal between 3T and 7T did not converge for neither the atlas-based approach nor the manually segmentation approach when quantified using the mean of crus cerebri as the background. However, using standard deviation of the background region as noise led to convergent estimates of NM-MRI CNR. While the mean of the background region has been used by several NM-MRI studies to define noise, CNR is typically defined as the ratio of mean of the signal to the standard deviation of the noise.

The choice of using standard deviation instead of the mean is based on the statistical properties of noise. Noise is often assumed to follow a Gaussian (normal) distribution with zero mean. In such cases, the standard deviation captures the spread or magnitude of the noise, which is a measure of the variations from the mean noise level. Using the standard deviation in the

denominator makes sense because it scales the CNR by the variability of the noise, which gives a better indication of the relative strength of the signal compared to the noise level. If the mean of the noise were used instead, it might not accurately reflect the variations and the true influence of the noise in the image, as the noise could have a mean value close to zero (which is often the case for Gaussian noise), but still have significant fluctuations.

For images segmented via an atlas, while the standard deviation formula yielded a significant rank order correlation between CNR estimates at 3T and 7T, the mean CNR value for 7T was drastically smaller than the mean CNR value for 3T. This could be because we used an atlas created at 3T to mask the images at 7T which was prompted by a dearth of midbrain atlases created from 7T brain images. As a rule of thumb, an atlas should have similar characteristics (e.g., field strength and resolution) to the target images. Using an atlas that does not match the target images can result in poor segmentation accuracy. Moreover, this can also increase the likelihood of partial volume effects — lower segmentation accuracy causing by mixed voxel intensities at tissue boundaries. Hence, it is important to have atlases that are as closely related (with respect of MRI properties) to target images as possible. With the increased availability and popularity of high field strength imaging, we hope that atlases that accurately delineate brain structures at 7T would be more accessible to researchers. Alternatively, automated (e.g., U-net; LeBerre et al., 2019) and deep learning algorithms (e.g., NigraNet; Gaurav et al., 2022) are becoming an increasingly popular choice amongst researchers for segmenting NM-MRI scans due to their cost and time-efficient nature. Establishing the validity of these tools for segmenting the SN is a valuable endeavour for future research in the field of NM imaging.

Co-registering 3T and 7T NM-MRI images presented the biggest challenge when employing the manual segmentation strategy. The two scanners have different orientations,

resolutions, and distortions due to the inherent differences in field strength. This makes it significantly harder to compare and/or integrating data across field strengths. As such, accounting for these differences is crucial for conducted a cross-compatibility analysis. In the present study, we used SPM-12 to co-register participant images at 3T with 7T. This was done to alleviate some of the aforementioned concerns by making the native space of the participants uniform across field strengths. The amount of movement required to co-register was quite significant. Furthermore, the amount of anatomical detail in binarized manually segmented masks is virtually non-existent. SPM-12 uses probability maps to characterize tissue types and identify neuroanatomical structures and the lack of detail makes it quite hard for a software like SPM-12 to successfully co-register images and masks with one another. Future research should explore the use of a more robust platforms such as Advanced Normalization Tools (ANTs) or automated machine learning software like Greedy within ITK-Snap for image registration.

We didn't observe an increase in CNR with an increase in magnetic field strength. This is contradictory to previous research. Several studies have found an increase in CNR with increasing field strength (Pohmann et al., 2016; Schäfer et al., 2008). In our sample, while contrast was higher for 7T (M = 214.80) than 3T (M = 209) to a certain extent, the increase in noise was disproportionately higher at 7T (M = 162.80) than 3T (M = 108*)*. Moreover, the distribution of the CC for 7T (SD = 40.78) was significantly more spread out than that at 3T (SD = 9.75). This problem was further exacerbated by the small sample size in our study. Variance and dispersion of the background distribution is directly related to noise in the data. Crucially, it decreases CNR. These findings may help explain the lack of field strength-based increase in CNR within our sample.

Contrary to findings from previous research (Xing et al., 2018), we did not find a significant decrease in NM with increasing age. In addition to the small sample size, the age range of participants in this study was also significantly narrower than that reported in Xing and colleagues (2018)'s research. Since the highest increase in NM content is mostly seen during childhood and adolescence, it is not surprising that we failed to find an effect of age on NM levels in our study. Replicating our study using a larger sample with a wider age range would afford us a better opportunity for examining such effects.

Aside from age and biological sex, no other demographic information was obtained from participants. NM levels within the brain can vary due to a variety of factors including medications (specifically dopamine antagonists and agonists), biological expression of enzymes e.g., tyrosinase (Jin et al., 2023), and the presence of psychiatric illnesses such as schizophrenia, depression, and psychotic disorders (Wengler et al., 2021). These factors should be statistically accounted for when calculating NM-MRI CNR to avoid confounding results.

Considering our results pertaining to the lower CNR value and higher noise levels at 7T, we recommend 3T MRI as a more suitable imaging tool for neuromelanin sensitive contrast. The choice between 7T and 3T MRI depends on the specific clinical or research. Higher magnetic field strength is not "universally" better than a lower field strength. Susceptibility to distortion induced artifacts, inhomogeneity of magnetic fields, and partial volume effects are some of the major limitations for 7T NM-MRI research. The SN is a small midbrain nucleus that is affected significantly by signal degradation factors. Within the context of NM-MRI, research has focused on the optimization of techniques and MRI acquisition parameters for 3T (Salzman et al.,2021; Wengler et al., 2020). Since ultra-high field strength imaging is still in its early stages of development, there is a lack of specialized protocols for image acquisition and contrast

enhancement. As ultra-high field strength imaging becomes more accessible and prevalent within research, hardware, sequences, and protocols would become increasingly sophisticated, advanced, and reliable. This would make it possible to achieve the best possible imaging quality and reduce challenges unique to high-field MRI.

References

Al Haddad, R., Chamoun, M., Tardif, C. L., Guimond, S., Horga, G., Rosa-Neto, P., & Cassidy, C. M. (2023). Normative Values of Neuromelanin-Sensitive MRI Signal in Older Adults Obtained Using a Turbo Spin Echo Sequence. *Journal of Magnetic Resonance Imaging*, *58*(1), 294–300. https://doi.org/10.1002/jmri.28530

Alamy, M., & Bengelloun, W. A. (2012). Malnutrition and brain development: An analysis of the effects of inadequate diet during different stages of life in rat. *Neuroscience and Biobehavioral Reviews, 36*(6), 1463–1480. https://doi.org/10.1016/j.neubiorev.2012.03.009

Berridge, K. C. (2004). Motivation concepts in behavioral neuroscience. *Physiology & Behavior, 81*(2), 179–209. https://doi.org/10.1016/j.physbeh.2004.02.004

Brake, W. G., Sullivan, R. M., & Gratton, A. (2000). Perinatal distress leads to lateralized medial prefrontal cortical dopamine hypofunction in adult rats. *The Journal of Neuroscience*, *20*(14), 5538–5543. https://doi.org/10.1523/JNEUROSCI.20-14-05538.2000

Cassidy, C. M., Carpenter, K. M., Konova, A. B., Cheung, V., Grassetti, A., Zecca, L., Abi-Dargham, A., Martinez, D., & Horga, G. (2020). Evidence for Dopamine Abnormalities in the Substantia Nigra in Cocaine Addiction Revealed by Neuromelanin-Sensitive MRI. *The American Journal of Psychiatry*, *177*(11), 1038–1047. https://doi.org/10.1176/appi.ajp.2020.20010090

Cassidy, C. M., Zucca, F. A., Girgis, R. R., Baker, S. C., Weinstein, J. J., Sharp, M. E., Bellei, C., Valmadre, A., Vanegas, N., Kegeles, L. S., Brucato, G., Kang, U. J., Sulzer, D., Zecca, L., Abi-Dargham, A., & Horga, G. (2019). Neuromelanin-sensitive MRI as a noninvasive proxy measure of dopamine function in the human brain. *Proceedings of the National Academy of Sciences of the United States of America*, *116*(11), 5108–5117. https://doi.org/10.1073/pnas.1807983116

Chen, X., Huddleston, D. E., Langley, J., Ahn, S., Barnum, C. J., Factor, S. A., Levey, A. I., & Hu, X. (2014). Simultaneous imaging of locus coeruleus and substantia nigra with a quantitative neuromelanin MRI approach. *Magnetic Resonance Imaging*, *32*(10), 1301–1306. https://doi.org/10.1016/j.mri.2014.07.003

Clancy, B., Darlington, R. B., & Finlay, B. L. (2001). Translating developmental time across mammalian species. *Neuroscience*, *105*(1), 7–17. https://doi.org/10.1016/s0306-4522(01)00171-3

Cowen D. (1986). The melanoneurons of the human cerebellum (nucleus pigmentosus cerebellaris) and homologues in the monkey. *Journal of Neuropathology and*

Experimental Neurology, *45*(3), 205–221. https://doi.org/10.1097/00005072-198605000-00001

DeMattei, M., Levi, A. C., & Fariello, R. G. (1986). Neuromelanic pigment in substantia nigra neurons of rats and dogs. *Neuroscience Letters*, *72*(1), 37–42. https://doi.org/10.1016/0304-3940(86)90614-2

Dunlop, B. W., & Nemeroff, C. B. (2007). The role of dopamine in the pathophysiology of depression. *Archives of General Psychiatry, 64*(3), 327–337. https://doi.org/10.1001/archpsyc.64.3.327

Dunn, J. P., Kessler, R. M., Feurer, I. D., Volkow, N. D., Patterson, B. W., Ansari, M. S., Li, R., Marks-Shulman, P., & Abumrad, N. N. (2012). Relationship of dopamine type 2 receptor binding potential with fasting neuroendocrine hormones and insulin sensitivity in human obesity. *Diabetes Care*, *35*(5), 1105–1111. https://doi.org/10.2337/dc11-2250

Egerton, A., Valmaggia, L. R., Howes, O. D., Day, F., Chaddock, C. A., Allen, P., Winton-Brown, T. T., Bloomfield, M., Bhattacharyya, S., Chilcott, J., Lappin, J. M., Murray, R. M., & McGuire, P. (2016). Adversity in childhood linked to elevated striatal dopamine function in adulthood. *Schizophrenia Research*, *176*(2-3), 171–176. https://doi.org/10.1016/j.schres.2016.06.005

Fallah, A.A., (2023). Evaluation of SN Volume Quantification Approaches using Neuromelanin-sensitive MRI (NM-MRI) [Unpublished master's thesis]. University of Western Ontario.

Gatzke-Kopp, L. M. (2011). The canary in the coalmine: the sensitivity of mesolimbic dopamine to environmental adversity during development. *Neuroscience and Biobehavioral Reviews*, *35*(3), 794–803. https://doi.org/10.1016/j.neubiorev.2010.09.013

Gaurav, R., Valabrègue, R., Yahia-Chérif, L., Mangone, G., Narayanan, S., Arnulf, I., Vidailhet, M., Corvol, J. C., & Lehéricy, S. (2022). NigraNet: An automatic framework to assess nigral neuromelanin content in early Parkinson's disease using convolutional neural network. *NeuroImage. Clinical*, *36*, 103250. https://doi.org/10.1016/j.nicl.2022.103250

Hartley, C. A., & Somerville, L. H. (2015). The neuroscience of adolescent decision-making. *Current Opinion in Behavioral Sciences, 5,* 108–115. https://doi.org/10.1016/j.cobeha.2015.09.004

Herrero, M. T., Hirsch, E. C., Kastner, A., Luquin, M. R., Javoy-Agid, F., Gonzalo, L. M., Obeso, J. A., & Agid, Y. (1993). Neuromelanin accumulation with age in catecholaminergic neurons from Macaca fascicularis brainstem. *Developmental Neuroscience*, *15*(1), 37–48. https://doi.org/10.1159/000111315

Isaias, I. U., Trujillo, P., Summers, P., Marotta, G., Mainardi, L., Pezzoli, G., Zecca, L., & Costa, A. (2016). Neuromelanin Imaging and Dopaminergic Loss in Parkinson's Disease. *Frontiers in Aging Neuroscience*, *8*, 196.

https://doi.org/10.3389/fnagi.2016.00196

Jin, W., Stehbens, S. J., Barnard, R. T., Blaskovich, M. A. T., & Ziora, Z. M. (2023). Dysregulation of tyrosinase activity: a potential link between skin disorders and neurodegeneration. *The Journal of Pharmacy and Pharmacology*, rgad107. Advance online publication. https://doi.org/10.1093/jpp/rgad107

Kemali, M., & Gioffré, D. (1985). Anatomical localisation of neuromelanin in the brains of the frog and tadpole. Ultrastructural comparison of neuromelanin with other melanins. *Journal of Anatomy*, *142*, 73–83.

Kerchner G. A. (2011). Ultra-high field 7T MRI: a new tool for studying Alzheimer's disease. *Journal of Alzheimer's Disease.*, *26 Suppl 3*, 91–95. https://doi.org/10.3233/JAD-2011-0023

Kim, H., Lee, D., & Kim, K. (2021). Combined Exposure to Metals in Drinking Water Alters the Dopamine System in Mouse Striatum. *International Journal of Environmental Research and Public Health*, *18*(12), 6558. https://doi.org/10.3390/ijerph18126558

Langley, J., Huddleston, D. E., Liu, C. J., & Hu, X. (2017). Reproducibility of locus coeruleus and substantia nigra imaging with neuromelanin sensitive MRI. *Magnetic Resonance Materials in Physics, Biology and Medicine*, *30*(2), 121–125. https://doi.org/10.1007/s10334-016-0590-z

Le Berre, A., Kamagata, K., Otsuka, Y., Andica, C., Hatano, T., Saccenti, L., Ogawa, T., Takeshige-Amano, H., Wada, A., Suzuki, M., Hagiwara, A., Irie, R., Hori, M., Oyama, G., Shimo, Y., Umemura, A., Hattori, N., & Aoki, S. (2019). Convolutional neural network-based segmentation can help in assessing the substantia nigra in neuromelanin MRI. *Neuroradiology*, *61*(12), 1387–1395. https://doi.org/10.1007/s00234-019-02279-w

Lee, T. W., Chen, C. Y., Chen, K., Tso, C. W., Lin, H. H., Lai, Y. L., Hsu, F. T., Chung, H. W., & Liu, H. S. (2021). Evaluation of the Swallow-Tail Sign and Correlations of Neuromelanin Signal with Susceptibility and Relaxations. *Tomography*, *7*(2), 107–119. https://doi.org/10.3390/tomography7020010

Li, H., Chen, Z., Gong, Q., & Jia, Z. (2020). Voxel-wise meta-analysis of task-related brain activation abnormalities in major depressive disorder with suicide behavior. *Brain Imaging and Behavior, 14*(4), 1298–1308. https://doi.org/10.1007/s11682-019-00045-3

Li, S. C., Lindenberger, U., & Bäckman, L. (2010). Dopaminergic modulation of cognition across the life span. *Neuroscience and Biobehavioral Reviews*, *34*(5), 625–630. https://doi.org/10.1016/j.neubiorev.2010.02.003

Magadza, T., & Viriri, S. (2021). Deep Learning for Brain Tumor Segmentation: A Survey of State-of-the-Art. *Journal of imaging*, *7*(2), 19. https://doi.org/10.3390/jimaging7020019

McArthur, S., McHale, E., Dalley, J. W., Buckingham, J. C., & Gillies, G. E. (2005). Altered mesencephalic dopaminergic populations in adulthood as a consequence of brief perinatal glucocorticoid exposure. *Journal of Neuroendocrinology, 17*(8), 475–482. https://doi.org/10.1111/j.1365-2826.2005.01331.x

McClure, S. M., York, M. K., & Montague, P. R. (2004). The neural substrates of reward processing in humans: the modern role of FMRI. *The Neuroscientist*, *10*(3), 260–268. https://doi.org/10.1177/1073858404263526

Monchi, O., Ko, J. H., & Strafella, A. P. (2006). Striatal dopamine release during performance of executive functions: A [(11)C] raclopride PET study. *NeuroImage*, *33*(3), 907–912. https://doi.org/10.1016/j.neuroimage.2006.06.058

Nakane, T., Nihashi, T., Kawai, H., & Naganawa, S. (2008). Visualization of neuromelanin in the Substantia nigra and locus ceruleus at 1.5T using a 3D-gradient echo sequence with magnetization transfer contrast. *Magnetic resonance in Medical Sciences*, *7*(4), 205–210. https://doi.org/10.2463/mrms.7.205

Pan, P., Zhan, H., Xia, M., Zhang, Y., Guan, D., & Xu, Y. (2017). Aberrant regional homogeneity in Parkinson's disease: A voxel-wise meta-analysis of resting-state functional magnetic resonance imaging studies. *Neuroscience and Biobehavioral Reviews*, *72*, 223–231. https://doi.org/10.1016/j.neubiorev.2016.11.018

Partridge, S. C., Singer, L., Sun, R., Wilmes, L. J., Klifa, C. S., Lehman, C. D., & Hylton, N. M. (2011). Diffusion-weighted MRI: influence of intravoxel fat signal and breast density on breast tumor conspicuity and apparent diffusion coefficient measurements. *Magnetic Resonance Imaging*, *29*(9), 1215–1221. https://doi.org/10.1016/j.mri.2011.07.024

Pohmann, R., Speck, O., & Scheffler, K. (2016). Signal-to-noise ratio and MR tissue parameters in human brain imaging at 3, 7, and 9.4 tesla using current receive coil arrays. *Magnetic Resonance in Medicine*, *75*(2), 801–809. https://doi.org/10.1002/mrm.25677

Pruessner, J. C., Champagne, F., Meaney, M. J., & Dagher, A. (2004). Dopamine Release in Response to a Psychological Stress in Humans and its Relationship to Early Life Maternal Care: A Positron Emission Tomography Study Using [^{11}C]Raclopride. *The Journal of Neuroscience, 24*(11), 2825–2831. https://doi.org/10.1523/JNEUROSCI.3422-03.2004

Qiu, Z., & Wang, J. (2021). A voxel-wise meta-analysis of task-based functional MRI studies on impaired gain and loss processing in adults with addiction. *Journal of Psychiatry & Neuroscience*, *46*(1), E128–E146. https://doi.org/10.1503/jpn.200047

Radwan, B., Liu, H., & Chaudhury, D. (2019). The role of dopamine in mood disorders and the associated changes in circadian rhythms and sleep-wake cycle. *Brain Research*, *1713*, 42–51. https://doi.org/10.1016/j.brainres.2018.11.031

Rangel-Barajas, C., Coronel, I., & Florán, B. (2015). Dopamine Receptors and Neurodegeneration. *Aging and Disease*, *6*(5), 349–368. https://doi.org/10.14336/AD.2015.0330

Rao, N. P., Jeelani, H., Achalia, R., Achalia, G., Jacob, A., Bharath, R. D., Varambally, S., Venkatasubramanian, G., & K Yalavarthy, P. (2017). Population differences in brain morphology: Need for population specific brain template. *Psychiatry Research: Neuroimaging*, *265*, 1–8. https://doi.org/10.1016/j.pscychresns.2017.03.018

Salzman, G., Kim, J., Horga, G., & Wengler, K. (2021). Standardized Data Acquisition for Neuromelanin-sensitive Magnetic Resonance Imaging of the Substantia Nigra. *Journal of Visualized Experiments : JoVE*, (175), 10.3791/62493. https://doi.org/10.3791/62493

Sasaki, M., Shibata, E., Tohyama, K., Takahashi, J., Otsuka, K., Tsuchiya, K., Takahashi, S., Ehara, S., Terayama, Y., & Sakai, A. (2006). Neuromelanin magnetic resonance imaging of locus ceruleus and substantia nigra in Parkinson's disease. *Neuroreport*, *17*(11), 1215–1218. https://doi.org/10.1097/01.wnr.0000227984.84927.a7

Schäfer, A., van der Zwaag, W., Francis, S. T., Head, K. E., Gowland, P. A., & Bowtell, R. W. (2008). High resolution SE-fMRI in humans at 3 and 7 T using a motor task. *Magnetic Resonance Materials in Physics, Biology and Medicine*, *21*(1-2), 113–120. https://doi.org/10.1007/s10334-007-0099-6

Sheu, Y. S., Polcari, A., Anderson, C. M., & Teicher, M. H. (2010). Harsh corporal punishment is associated with increased T2 relaxation time in dopamine-rich regions. *NeuroImage*, *53*(2), 412–419. https://doi.org/10.1016/j.neuroimage.2010.06.043

Sinclair, D., Purves-Tyson, T. D., Allen, K. M., & Weickert, C. S. (2014). Impacts of stress and sex hormones on dopamine neurotransmission in the adolescent brain. *Psychopharmacology*, *231*(8), 1581–1599. https://doi.org/10.1007/s00213-013-3415-z

Sulzer, D., Bogulavsky, J., Larsen, K. E., Behr, G., Karatekin, E., Kleinman, M. H., Turro, N., Krantz, D., Edwards, R. H., Greene, L. A., & Zecca, L. (2000). Neuromelanin biosynthesis is driven by excess cytosolic catecholamines not accumulated by synaptic vesicles. *Proceedings of the National Academy of Sciences of the United States of America*, *97*(22), 11869–11874. https://doi.org/10.1073/pnas.97.22.11869

Sulzer, D., Cassidy, C., Horga, G., Kang, U. J., Fahn, S., Casella, L., Pezzoli, G., Langley, J., Hu, X. P., Zucca, F. A., Isaias, I. U., & Zecca, L. (2018). Neuromelanin detection by magnetic resonance imaging (MRI) and its promise as a biomarker for Parkinson's disease. *NPJ Parkinson's Disease*, *4*, 11. https://doi.org/10.1038/s41531-018-0047-3

Sung, Y. H., Noh, Y., & Kim, E. Y. (2021). Early-stage Parkinson's disease: Abnormal nigrosome 1 and 2 revealed by a voxelwise analysis of neuromelanin-sensitive MRI. *Human Brain Mapping*, *42*(9), 2823–2832. https://doi.org/10.1002/hbm.25406

Susser, E., St Clair, D., & He, L. (2008). Latent effects of prenatal malnutrition on adult health: the example of schizophrenia. *Annals of the New York Academy of Sciences*, *1136*, 185–192. https://doi.org/10.1196/annals.1425.024

Trujillo, P., Summers, P. E., Ferrari, E., Zucca, F. A., Sturini, M., Mainardi, L. T., Cerutti, S., Smith, A. K., Smith, S. A., Zecca, L., & Costa, A. (2017). Contrast mechanisms associated with neuromelanin-MRI. *Magnetic Resonance in Medicine*, *78*(5), 1790–1800. https://doi.org/10.1002/mrm.26584

van der Pluijm, M., Cassidy, C., Zandstra, M., Wallert, E., de Bruin, K., Booij, J., de Haan, L., Horga, G., & van de Giessen, E. (2021). Reliability and Reproducibility of Neuromelanin-Sensitive Imaging of the Substantia Nigra: A Comparison of Three Different Sequences. *Journal of Magnetic Resonance Imaging*, *53*(3), 712–721. https://doi.org/10.1002/jmri.27384

Wang, L., Yan, Y., Zhang, L., Liu, Y., Luo, R., & Chang, Y. (2021). Substantia nigra neuromelanin magnetic resonance imaging in patients with different subtypes of Parkinson disease. *Journal of Neural Transmission*, *128*(2), 171–179. https://doi.org/10.1007/s00702-020-02295-8

Wang, X., Huang, P., Haacke, E. M., Liu, Y., Zhang, Y., Jin, Z., Li, Y., Xu, Q., Liu, P., Chen, S., He, N., & Yan, F. (2023). Locus coeruleus and substantia nigra neuromelanin magnetic resonance imaging differentiates Parkinson's disease and essential tremor. *NeuroImage. Clinical*, *38*, 103420. https://doi.org/10.1016/j.nicl.2023.103420

Wengler, K., Ashinoff, B. K., Pueraro, E., Cassidy, C. M., Horga, G., & Rutherford, B. R. (2021). Association between neuromelanin-sensitive MRI signal and psychomotor slowing in late-life depression. *Neuropsychopharmacology*, *46*(7), 1233–1239. https://doi.org/10.1038/s41386-020-00860-z

Wengler, K., He, X., Abi-Dargham, A., & Horga, G. (2020). Reproducibility assessment of neuromelanin-sensitive magnetic resonance imaging protocols for region-of-interest and voxelwise analyses. *NeuroImage*, *208*, 116457. https://doi.org/10.1016/j.neuroimage.2019.116457

Wieland, L., Fromm, S., Hetzer, S., Schlagenhauf, F., & Kaminski, J. (2021). Neuromelanin-Sensitive Magnetic Resonance Imaging in Schizophrenia: A Meta-Analysis of Case-Control Studies. *Frontiers in Psychiatry*, *12*, 770282. https://doi.org/10.3389/fpsyt.2021.770282

Wu, W., Lu, Y., Mane, R., & Guan, C. (2020). Deep Learning for Neuroimaging Segmentation with a Novel Data Augmentation Strategy. *Annual International Conference of the IEEE Engineering in Medicine and Biology Society, 2020*, 1516–1519. https://doi.org/10.1109/EMBC44109.2020.9176537

Xing, Y., Sapuan, A. H., Martín-Bastida, A., Naidu, S., Tench, C., Evans, J., Sare, G., Schwarz, S. T., Al-Bachari, S., Parkes, L. M., Kanavou, S., Raw, J., Silverdale, M., Bajaj, N., Pavese, N., Burn, D., Piccini, P., Grosset, D. G., & Auer, D. P. (2022). Neuromelanin-MRI to Quantify and Track Nigral Depigmentation in Parkinson's Disease: A Multicenter Longitudinal Study Using Template-Based Standardized Analysis. *Movement Disorders*, *37*(5), 1028–1039. https://doi.org/10.1002/mds.28934

Xing, Y., Sapuan, A., Dineen, R.A. and Auer, D.P. (2018), Life span pigmentation changes of the substantia nigra detected by neuromelanin-sensitive MRI. *Movement Disorders, 33*(11), 1792-1799. https://doi.org/10.1002/mds.27502

Yeragani, V. K., Tancer, M., Chokka, P., & Baker, G. B. (2010). Arvid Carlsson, and the story of dopamine. *Indian Journal of Psychiatry*, *52*(1), 87–88. https://doi.org/10.4103/0019-5545.58907

Zecca, L., Casella, L., Albertini, A., Bellei, C., Zucca, F. A., Engelen, M., Zadlo, A., Szewczyk, G., Zareba, M., & Sarna, T. (2008). Neuromelanin can protect against iron-mediated oxidative damage in system modeling iron overload of brain aging and Parkinson's disease. *Journal of Neurochemistry*, *106*(4), 1866–1875. https://doi.org/10.1111/j.1471-4159.2008.05541.x

Zecca, L., Costi, P., Mecacci, C., Ito, S., Terreni, M., & Sonnino, S. (2000). Interaction of human substantia nigra neuromelanin with lipids and peptides. *Journal of Neurochemistry*, *74*(4), 1758–1765. https://doi.org/10.1046/j.1471-4159.2000.0741758.x

Zecca, L., Wilms, H., Geick, S., Claasen, J. H., Brandenburg, L. O., Holzknecht, C., Panizza, M. L., Zucca, F. A., Deuschl, G., Sievers, J., & Lucius, R. (2008). Human neuromelanin induces neuroinflammation and neurodegeneration in the rat substantia nigra: implications for Parkinson's disease. *Acta Neuropathologica*, *116*(1), 47–55. https://doi.org/10.1007/s00401-008-0361-7

Zucca, F. A., Basso, E., Cupaioli, F. A., Ferrari, E., Sulzer, D., Casella, L., & Zecca, L. (2014). Neuromelanin of the human substantia nigra: an update. *Neurotoxicity Research*, *25*(1), 13–23. https://doi.org/10.1007/s12640-013-9435-y

Zucca, F. A., Giaveri, G., Gallorini, M., Albertini, A., Toscani, M., Pezzoli, G., Lucius, R., Wilms, H., Sulzer, D., Ito, S., Wakamatsu, K., & Zecca, L. (2004). The neuromelanin of human substantia nigra: physiological and pathogenic aspects. *Pigment Cell Research*, *17*(6), 610–617. https://doi.org/10.1111/j.1600-0749.2004.00201.x

Zucca, F. A., Vanna, R., Cupaioli, F. A., Bellei, C., De Palma, A., Silvestre, D. D., Mauri, P., Grassi, S., Prinetti, A., Casella, L., Sulzer, D., & Zecca, L. (2018). Neuromelanin organelles are specialized autolysosomes that accumulate undegraded proteins and lipids in aging human brain and are likely involved in Parkinson's disease. *NPJ Parkinson's Disease, 4*, 1-23. http://doi.org/10.1038/s41531-018-0050-8

LAIBA RIZWAN

EDUCATION

M.Sc. in Neuroscience *2021/Sept*
University of Western Ontario *2023/Aug*
Quantifying Neuromelanin Across Varying Magnetic Field Strengths
Advisor: J. Bruce Morton, Ph.D.

Honours B.Sc. in Psychology (High Distinction) *2017/Sep*
University of Toronto, Scarborough *2021/Jun*

RESEARCH EXPERIENCE

Undergraduate Honours Thesis with Prof. Kosha Bramesfeld *2020/Jun*
Department of Psychology | University of Toronto Scarborough *2021/Apr*
Project: *"Educational Games as a Pedagogical Tool for Disability Awareness"*

- Designed and conducted participatory research to capture an authentic picture of the disability experiences
- Conducted thematic analysis of qualitative data and proposed mechanisms of change and suggestions for reform

Research Assistant (Supervised Study) with Prof. Michael Best *2019/Sep*
Department of Psychology | University of Toronto Scarborough *2020/Apr*
Project: *"Ostracism Towards individuals with Schizophrenia*

- Designed and conducted the experimental protocol for the study in the capacity of a student principal investigator
- Collected electrophysiological (EEG), behavioural, and questionnaire data
- Performed statistical analyses using SPSS

Clinical Research Assistant with Dr. Russell Schachar *2019/May*
Department of Psychiatry | The Hospital for Sick Children *2021/Aug*

- Conducting clinical assessments and administering neuropsychological tests to children with ADHD, OCD and Tourette Syndrome including

Clinical Research Trainee with Dr. Brendan Andrade *2019/Oct*
Better Behaviours Team | Centre for Addiction and Mental Health (CAMH) *2020/Feb*

- Administered the Cambridge Neuropsychological Test Automated Battery (CANTAB) to children (7-12 yrs.) with a diagnosis of conduct disorders
- Managed health records using REDCap
- Assisted with collection and analysis of physiological data

Undergraduate Research Assistant with Prof. Laura Cirelli *2019/May - 2019/Aug*
Department of Psychology | University of Toronto Scarborough

- Involved in recruitment, data collection and analysis
- Assisted in organizing Baby Opera field experiment conducted offsite at McMaster University

Project Assistant with Prof. Konstatine Zakzanis *2019/Mar*
Department of Psychology | University of Toronto Scarborough

- Conducted a systematic literature review for the project "Apathy in Traumatic Brain Injury" using a variety of databases
- Developed proficiency in the use of PsycINFO (ProQuest & Ovid), PubMed, Google Scholar, Scopus, and Web of Science

HONOURS AND AWARDS

UTSC Dean's List (top 10% students) *2018- 2021*
UTSC Psychology Travel Award *2021*
Psi Chi International Honour Society in Psychology *2019*
York University World Scholars Program Scholarship ($20,000) *2017*

PUBLICATIONS

Accepted Book Chapter

Rizwan, L., Bramesfeld, K.D., & Taddeo, M. (in press) Rethinking the Classroom as a Hub for Intellectual Joy and Scholastic Passion: A Dialogue. In M. Feifer, M. L. Butler & J. Davis-McElligatt (Eds.), *Transgressive Teaching & Learning: Critical Essays on bell hooks' Engaged Pedagogy*

Manuscripts Under Review

Zahid, A., **Rizwan, L.,** Taylor, G. J., Lau, S. C. L., & Bagby, R. M. (2022). *Development of a revised version of the Urdu translation of the 20-item Toronto Alexithymia Scale* [Manuscript submitted for publication]. Department of Psychology, University of Toronto Scarborough.

Manuscripts in Progress

Zahid, A., **Rizwan, L.,** Cheema, A. A., & Bagby, R. M. (in prep). *Urdu translation and validation of the Personality Inventory for DSM-5 (PID-5)*. Department of Psychology, University of Toronto Scarborough.

Zahid, A., Cheema, A. A., **Rizwan, L.,** Zahid, M. M., & Bagby, R. M. (in prep). *Unpacking culture from language in the cross-validation of the Personality Inventory for DSM-5 (PID-5) in an Urdu-speaking sample*. Department of Psychology, University of Toronto Scarborough.

TALKS AND POSTER PRESENTATIONS

Rizwan, L., Fallah, A., Kitzler, H.H., Hösel, L. & Morton, J.B. (2023, July 22 - 25). *Characterizing the Volume & NM Content Measures of the Substantia Nigra: A Comparison between 3T and 7T Neuromelanin-Sensitive MRI* [Poster session]. OHBM 2023, Montreal, QC, Canada

Bramesfeld, K.D., **Rizwan, L.,** Abeid, S., Mehta, A., Bhatia, D., & Thayaparan, D. (2021, May 12-14). Voices of Lived Experience: *Working with students-as-partners to Develop Inclusive and Authentic Learning Content Awareness* [Conference session]. 14th Annual University of Toronto Teaching and Learning Symposium, Toronto, ON, Canada

Rizwan, L. & Bramesfeld, K.D. (2021, May 13- 14). Stories of Thriving & Surviving: *Using a Participatory Research Design to inform Pedagogical Tools for Disability Awareness* [Poster session]. Interdisciplinary Conference in Psychology 2021, Ottawa, ON, Canada

PROFESSIONAL DEVELOPMENT

Teaching Assistant Training Program *2021/Sep*
Centre for Teaching & Learning | University of Western Ontario

- A 20-hour interdisciplinary Course for Graduate Teaching Assistants on the strategies and practice of University Teaching e.g., fair grading practices, lesson design, and giving feedback

Teaching Mentor Program *2021/Oct*
Centre for Teaching & Learning | University of Western Ontario *2021/Dec*

- A cohort-based hands-on learning experience involving groups of interdisciplinary graduate students and postdoctoral scholars to observe and offer feedback on one another's teaching

Future Prof Series
Centre for Teaching & Learning | University of Western Ontario

- Developing Your Teaching Dossier *2021/Feb*
- Decentering English in the Classroom *2021/Mar*
- Leadership in Wellness *2022/Oct*
    - *Part 1: Cultivating Student Mental Health*
    - Part 2: *Initiating Mental Health Conversations with your Students*

EDUCATIONAL LEADERSHIP EXPERIENCE

Associate Editor | Undergraduate Research in Natural and Clinical Science and Technology Journal — *2022/Oct - 2023/Jan*

- Guiding and mentoring undergraduate students in designing, developing, and writing a full-length study protocol or review

Graduate Mentor | Women in Science Mentorship Program — *2022/Oct - 2023/Mar*

- Mentoring upper year female undergraduate students in STEM fields
- Attending social events to foster a sense of community and belongingness amongst women in science
- Providing one-on-one guidance and support to mentees for navigating academia, skill building, finding work-life balance, managing stress, and making informed career choices

Member, Organization Committee | Brainhack Western' 22 — *2022/ Nov-2022/Dec*

- Assisted with the organization of Brainhack Western: An annual event that aims to bring together researchers and trainees with disparate backgrounds to collaborate on open science projects in neuroimaging and neuroscience.

Graduate Program Reviewer | Canadian Medical Hall of Fame — *2022/Apr*

- Reviewed existing program content of a six-session, teacher-led senior elementary school program in neuroscience for science accuracy, simplicity, and continuity
- Provided feedback and identified opportunities for improvement
- Proposed engaging hands-on activities for promoting knowledge retention

Poster Judge | Inspiring Diversity in STEM Research Conference — *2022/Mar*

- Evaluated the quality of posters presented at the conference
- Provided presenters with actionable feedback and suggestions for improvement

President | Psi Chi, The International Honor Society in Psychology — *2020/Nov 2021/Apr*

- Chaired the executive committee
- Organized and oversaw chapter- related Psi Chi programs
- Acted as a liaison with other campus and departmental organizations
- Assisted the faculty advisor in the induction ceremony and annual membership drives

Undergraduate Peer Reviewer | Journal of Natural Sciences — *2020/May - 2021/May*

- Collaborated with the senior undergraduate reviewer to edit and

provide constructive feedback on the articles submitted for publication in the journal

Cognitive Neuroscience Instructor | The Neuroscience Fellowship *2020/Jun - 2020/Sep*

- Created lecture materials and taught neuroscience-based content to prospective neuroscience students. Topics include cognitive neuroscience of attention, neuropsychological sequalae of traumatic brain injury

SUMMARY OF COURSES TAUGHT

Graduate Teaching Assistant | University of Western Ontario

Course	Description	Term
PSYCHOL 1002 A	Intro to Psychology as a Natural Science	Fall'21
PSYCHOL 1003 B	Intro to Psychology as a Social Science	Winter' 22
PSYCHOL 3485 A	Research in Developmental Cognitive Neuroscience	Fall' 22
PSYCHOL 2812	Statistics for Psychology II	Winter' 23

COMMUNITY SERVICE AND LEADERSHIP EXPERIENCE

Crisis Line Responder | Distress Centres of Greater Toronto *2018/Dec - 2019/Dec*

- Provided community and mental health resources and crisis intervention to service users from a variety of different clinical populations including mood and neuro-degenerative disorders
- Applied a solution-focused model to encourage problem solving and rapport building

Public Relations Director | Connect 4 Life, Mississauga, Canada *2018/May - 2019/May*

- Generated plans and made decisions to support organizational development and representation
- Fundraised to remove barriers for individuals with disabilities

PROFESSIONAL CONFERENCES ATTENDED

Organization for Human Brain Mapping Conference (OHBM 2023) *2023/Jul*
UTSC Library Undergraduate Research Forum *2021/Apr*
14th Annual University of Toronto Teaching and Learning Symposium *2021/May*
51st Annual Ontario Psychology Undergraduate Thesis Conference *2021/Jun*